

Enhancing the Dynamic Range of Targeted Energy Transfer in Acoustics Using Several Nonlinear Membrane Absorbers

R. Bellet^a, B. Cochelin^{b,*}, R. Côte^c, P.-O. Mattei^a

^a*CNRS-LMA, UPR 7051, F-13402 Marseille Cedex 20, France*

^b*École Centrale Marseille, CNRS-LMA UPR 7051, F-13451 Marseille Cedex, France*

^c*Aix-Marseille Univ, CNRS-LMA UPR 7051, F-13402 Marseille Cedex 20, France*

Abstract

In order to enhance the robustness and the energy range of efficiency of targeted energy transfer (TET) phenomena in acoustics, we discuss in this paper about the use of multiple nonlinear membrane absorbers in parallel. We show this way, mainly thanks to an experimental set-up with two membranes, that the different absorbers have additional effects that extend the efficiency and the possibilities of observation of TET. More precisely, we present the different behavior of the system under sinusoidal forcing and free oscillations, characterizing the phenomena for all input energies. The frequency responses are also presented, showing successive clipping of the original resonance peak of the system. A model is finally used to generalize these results to more than two NES and to simulate the case of several very similar membranes in parallel which shows how to extend the existence zone of TET.

1. Introduction

It has been shown that the use of nonlinear absorber (or nonlinear energy sink) in the field of passive vibration control can provide very interesting results, exploiting the targeted energy transfer (TET) phenomenon. The principle is to couple together a primary system and a nonlinear energy sink (NES) in order to achieve an irreversible transfer of energy towards the absorber. The dynamics of such a system differs dramatically from those of linear absorbers and have been described in details in [1, 2, 3, 4, 5] in terms of resonance capture and nonlinear normal modes. A lot of papers have been published about different cases of linear system (a wave guide [6], a rod [7, 8, 9], a beam [10], a plate [11], a chain of coupled linear oscillators [12]) and different applications (seismic mitigation [13, 14], aeroelastic instabilities control [15, 16] or drill-string systems stabilization [17]). For applications to Acoustics, the possibility of using a NES (composed by a thin circular viscoelastic membrane) coupled to an acoustic medium was demonstrated in [18, 19] as a new technique of passive noise control in the low frequency domain where no efficient dissipative mechanism exists.

*corresponding author.

Email addresses: bellet@lma.cnrs-mrs.fr (R. Bellet), bruno.cochelin@ec-marseille.fr (B. Cochelin), cote@lma.cnrs-mrs.fr (R. Côte), mattei@lma.cnrs-mrs.fr (P.-O. Mattei)

In every case, one of the drawbacks of targeted energy transfer mechanism is the existence of limited energy range in which the NES has its maximal efficiency. In order to enhance this range, it has been demonstrated in [20, 21] that the use of several NES could be a good solution. As in most papers about TET, the considered system is mechanical and the configuration is the nongrounded one, where the NES is only attached to the primary system, via a nonlinear stiffness. The authors showed that the most efficient configuration for the multiple NES is a series coupling, as a parallel coupling creates problems of additional mass effect. Indeed, in a nongrounded configuration, the NES has to be as light as possible. In the case of controlling an acoustic medium, the only possible configuration is grounded (the membrane has to be attached to a wall), the additional mass effect is not a problem and a parallel NES configuration is easier to build than a series one. We therefore chose to work on the use of several nonlinear membrane absorbers in parallel to control an acoustic primary system in order to enhance the robustness and the dynamic range of TET phenomena.

In this study, we begin with measurements of the response of a 2 NES system. The NES have very different activation thresholds, which permits their individual monitoring. Then we simulate similar systems, with 2 or 4 membranes. Then we simulate a different situation where NES properties are very close, and we analyze our results. The paper is organized as follows : first we present the setup and the calculation model. Then we present and analyze measurements made with 3 different excitation regimes : sine source, free oscillations, and swept sine source. The third part is devoted to numerical simulations, and then we conclude.

2. Experimental study

2.1. Experimental set-up

The experimental set-up is based on the set-up presented in [19], with an acoustic source made of a loudspeaker and a box, a primary acoustic system based on the first mode of an open tube and a nonlinear absorber made of a thin circular visco-elastic membrane, coupled to the tube by a coupling box. As the acoustic pressure is spatially uniform in the coupling box, the side on which the membrane is settled does not matter. We thus used one of the free faces of this box to add a second membrane, leading to a configuration with two nonlinear membrane absorbers in parallel. Except for this second membrane, the set-up is identical to the one fully described in reference [19]. Two displacement sensors (laser triangulation) are used to measure the displacement of the center of the membranes (see Fig. 1). The displacements are positives for inward movements of the membranes.

The model associated to the set-up is also the same than the previous one, with an additional membrane equation, leading to a three degrees of freedom (3dof) system:

$$\begin{aligned} m_a \ddot{u} + c_f \dot{u} + k_a u + S_t k_b (S_t u - \frac{S_1}{2} q_1 - \frac{S_2}{2} q_2) &= F \cos(\Omega t) \\ m_1 \ddot{q}_1 + k_{11} [(\frac{f_{11}}{f_{01}})^2 q_1 + \eta_1 \dot{q}_1] + k_{31} [q_1^3 + 2\eta_1 q_1^2 \dot{q}_1] + \frac{S_1}{2} k_b (\frac{S_1}{2} q_1 + \frac{S_2}{2} q_2 - S_t u) &= 0 \\ m_2 \ddot{q}_2 + k_{12} [(\frac{f_{12}}{f_{02}})^2 q_2 + \eta_2 \dot{q}_2] + k_{32} [q_2^3 + 2\eta_2 q_2^2 \dot{q}_2] + \frac{S_2}{2} k_b (\frac{S_1}{2} q_1 + \frac{S_2}{2} q_2 - S_t u) &= 0 \end{aligned}$$



Figure 1: Experimental set-up with two membrane absorbers.

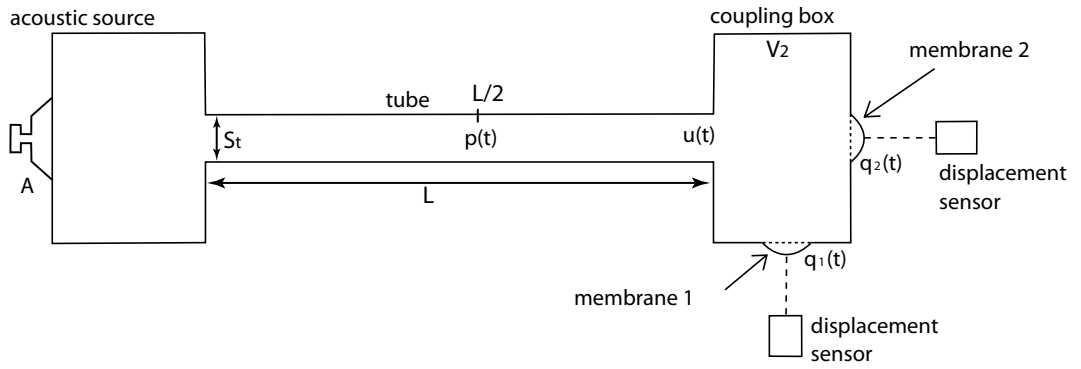


Figure 2: Scheme of the experimental set-up with two membrane absorbers. \mathcal{A} : amplitude voltage of the sinusoidal input signal. $p(t)$: acoustic pressure at the middle of the tube. $u(t)$: air displacement at the end of the tube. $q_1(t)$ and $q_2(t)$: respective displacements of the centers of the membranes 1 and 2.

$$\begin{aligned}
\text{with } m_a &= \frac{\rho_a S_t L}{2}, \quad m_i = \frac{\rho_m h S_i}{3}, \quad k_b = \frac{\rho_a c_0^2}{V_2}, \quad k_a = \frac{\rho_a S_t c_0^2 \pi^2}{2L} \\
k_{1i} &= \frac{1.015^4 \pi^5}{36} \frac{E h_i^3}{(1 - \nu^2) R_i^2}, \quad k_{3i} = \frac{8\pi E h_i}{3(1 - \nu^2) R_i^2} \\
f_{0i} &= \frac{1}{2\pi} \sqrt{\frac{1.015^4 \pi^4}{12} \frac{E h_i^2}{(1 - \nu^2) \rho_m R_i^4}}, \quad S_i = \pi R_i^2
\end{aligned}$$

In that system, the 3dof are the three displacements $u(t)$, $q_1(t)$, $q_2(t)$ of the air at the end of the tube and the center of the membranes M_1 and M_2 respectively. The other parameters are:

$\rho_a = 1.3 \text{ kg.m}^{-3}$	density of the air
$S_t = 6.9 \times 10^{-3} \text{ m}^2$	section of the tube
$L = 2 \text{ m}$	length of the tube
$\rho_m = 980 \text{ kg.m}^{-3}$	density of the membranes
$h_1 = 0.18 \text{ mm}$	thickness of M_1
$h_2 = 0.39 \text{ mm}$	thickness of M_2
$R_1 = 20 \text{ mm}$	radius of M_1
$R_2 = 30 \text{ mm}$	radius of M_2
$S_1 = 1.3 \times 10^{-3} \text{ m}^2$	surface of M_1
$S_2 = 2.8 \times 10^{-3} \text{ m}^2$	surface of M_2
$f_{11} = 59 \text{ Hz}$	first resonance frequency of M_1 with a certain pre-stress
$f_{12} = 47 \text{ Hz}$	first resonance frequency of M_2 with a certain pre-stress
f_{0i}	first resonance frequency of M_i without pre-stress
$E = 1.48 \text{ MPa}$	Young modulus of the membranes
$\nu = 0.49$	Poisson's ratio of the membranes
η_i	damping factor of M_i
F	amplitude of the excitation term
$V_2 = 27 \times 10^{-3} \text{ m}^3$	volume of the coupling box

The different energies are then given by:

$$\begin{aligned}
E_{tube} &= \frac{1}{2} m_a \dot{u}^2 + \frac{1}{2} k_a u^2 \\
E_{membranes} &= \frac{1}{2} m_1 \dot{q}_1^2 + \frac{1}{2} k_{11} \left(\frac{f_{11}}{f_{01}} \right)^2 q_1^2 + \frac{1}{4} k_{31} q_1^2 + \frac{1}{2} m_2 \dot{q}_2^2 + \frac{1}{2} k_{12} \left(\frac{f_{12}}{f_{02}} \right)^2 q_2^2 + \frac{1}{4} k_{32} q_2^2 \\
E_{coupling \text{ box}} &= \frac{1}{2} k_b \left(S_t u - \frac{S_1}{2} q_1 - \frac{S_2}{2} q_2 \right)^2 \\
E_{total} &= E_{tube} + E_{membranes} + E_{couplingbox}
\end{aligned}$$

2.2. Regimes under sinusoidal excitation

The acoustic medium, composed by an open tube, has its first resonance at 89 Hz. As the aim of the membrane absorbers is to reduce this resonance, we describe the system behavior under sinusoidal excitation at the first resonance frequency of the acoustic medium. The figures from 3(a) to 3(e) show the time series observed experimentally with this excitation for a increasing input amplitude \mathcal{A} using a small and thin membrane (membrane M_1 : $h_1 = 0.18 \text{ mm}$, $R_1 = 2 \text{ cm}$, $f_{11} = 59 \text{ Hz}$) and another larger and thicker (membrane M_2 : $h_2 = 0.39 \text{ mm}$, $R_2 = 3 \text{ cm}$, $f_{12} = 47 \text{ Hz}$).

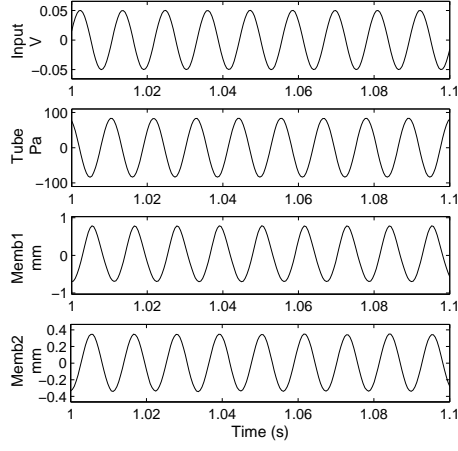
The system behavior can be described using the following steps, which define at the same time the first and second activation thresholds $S_1^{M_i}$ and $S_2^{M_i}$ of the membrane M_i :

- $\mathcal{A} < S_1^{M_1}$ (Fig. 3(a)): sinusoidal regime where none of the two membranes is activated, both vibrating in opposite phase with the displacement at the end of the tube.
- $S_1^{M_1} < \mathcal{A} < S_2^{M_1}$ (Fig. 3(b)): Activation of the first membrane leading to the quasi-periodic regime we already discussed in [19] involving the acoustic medium and the membrane M_1 , the membrane M_2 remaining inactive and passively following the vibration inside the tube. During this quasi-periodic regime, each time the membrane M_1 is activated, a resonance capture occurs with the acoustic medium (the displacement of the membrane is in phase with the displacement at the end of the tube) and a targeted energy transfer is created from this linear primary system to the NES.
- $S_2^{M_1} < \mathcal{A} < S_1^{M_2}$ (Fig. 3(c)): beyond the threshold $S_2^{M_1}$, the regime is periodic and the membrane M_1 vibrates with a large amplitude and in phase with the displacement at the end of the tube, while the membrane M_2 is still inactive and remains out of phase with this last degree of freedom. So far, behaviors are exactly the same as those observed with a single membrane set-up in [19].
- $S_1^{M_2} < \mathcal{A} < S_2^{M_2}$ (Fig. 3(d)): activation of the membrane M_2 leading to a second quasi-periodic regime involving the acoustic medium and the membrane M_2 , while the membrane M_1 preserves its periodic evolution (barely disturbed by the quasiperiodic regime that exists around it).
- $\mathcal{A} > S_2^{M_2}$ (Fig. 3(e)): beyond the last threshold $S_2^{M_2}$, the regime is periodic again and the membrane M_2 also vibrates with a large amplitude and in phase with the displacement at the end of the tube and the membrane M_1 . Within this last regime, both membranes are on a resonance capture with the acoustic medium.

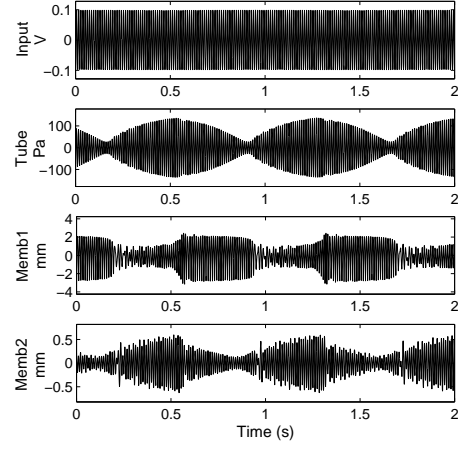
Basically, these steps correspond to the successive activation of the different membranes, each one corresponding to the same phenomena as those observed with a single membrane set-up. Note that these mechanisms, where $S_2^{M_1} < S_1^{M_2}$, with clearly separated phases is a consequence of two very different membrane configurations (radius, thickness and pre-stress). For practical experimental limitations, the case of very close membrane configurations couldn't be studied on this set-up. This case will be discussed further in this paper thanks to simulations.

2.3. Free oscillations

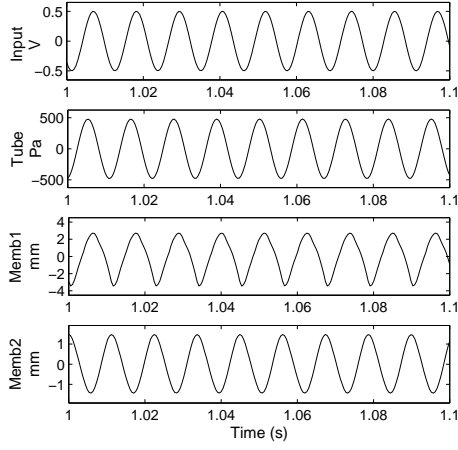
The figures from 4(a) to 4(c) show the different types of free oscillations observed with these two membranes, after a sinusoidal excitation at 89 Hz suddenly stopped, for increasing values of initial input level. These figures include a diagram showing the evolution of the percentage of energy present in the acoustic medium and in both membranes. Wavelet transforms are also presented, in order to observe the temporal evolution of the frequency of the different time series. A description of the observed phenomena can be summarized as follows:



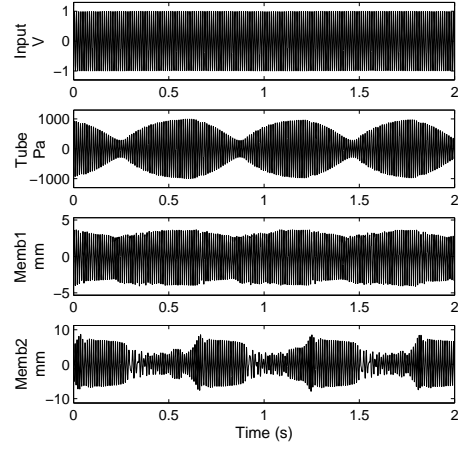
(a) $\mathcal{A} = 0.05 \text{ V}$.



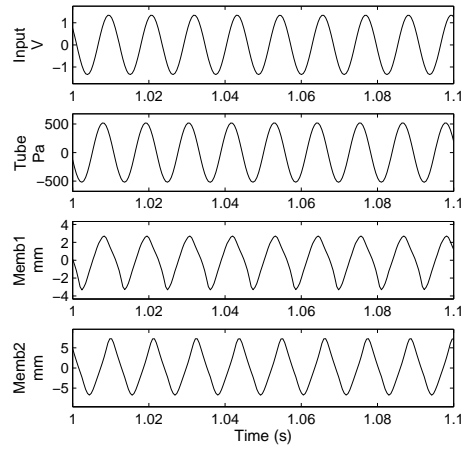
(b) $\mathcal{A} = 0.1 \text{ V}$.



(c) $\mathcal{A} = 0.5 \text{ V}$.



(d) $\mathcal{A} = 1 \text{ V}$.



(e) $\mathcal{A} = 1.4 \text{ V}$.

Figure 3: *Experimental results*. Oscillations of the system under sinusoidal excitation with different amplitudes and constant frequency (89 Hz). From top to bottom: sinusoidal input signal, acoustic pressure at the middle of the tube, displacement of the center of the membrane M_1 and displacement of the center of the membrane M_2 .

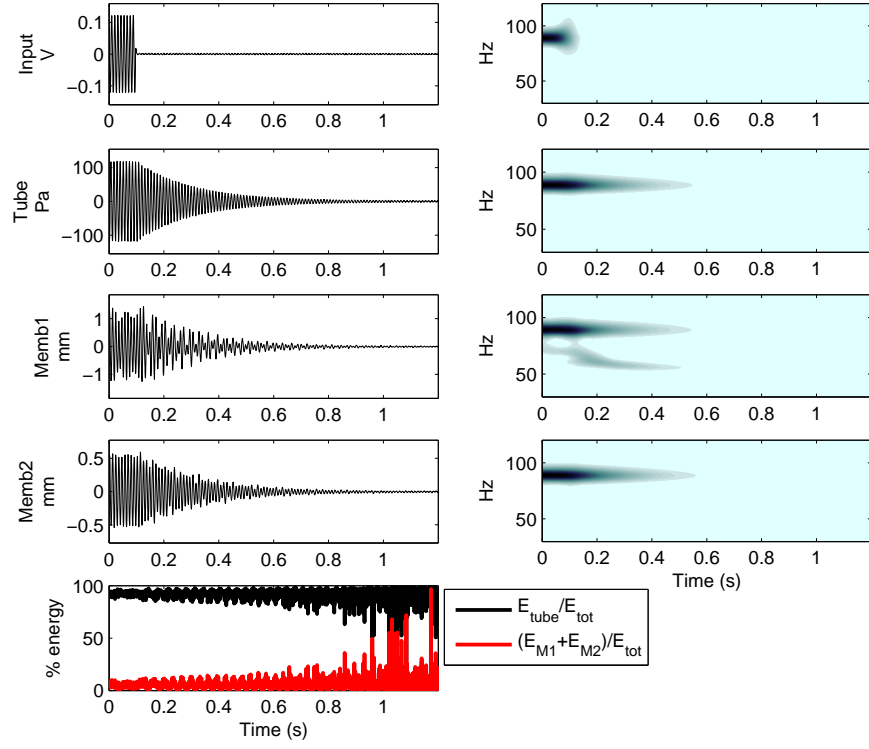
- $\mathcal{A} < S_1^{M_1}$ (Fig. 4(a)) : for low initial energy conditions, the membranes are not initially active and the decrease of the acoustic pressure is classically exponential. The energy remains always localized in the acoustic medium and the spectrum of the membranes movements mainly reflects a single component at the acoustic resonance frequency, the membranes just following passively the acoustic vibration.
- $S_2^{M_1} < \mathcal{A} < S_1^{M_2}$ (Fig. 4(b)) : beyond the second activation threshold of the membrane M_1 , and below the first threshold of the membrane M_2 , a targeted energy transfer occurs from the acoustic medium to the membrane M_1 and we observe an almost linear decrease similar to what we observed previously with a single membrane set-up. Indeed, since the membrane M_2 is not activated, it has no influence on the rest of the system and observations correspond to what has been seen so far in [19]. The energy diagram clearly shows how fast the energy is localized on the membrane, from the initial instant of free oscillations. After the transfer, the energy remains always localized on the membrane: the transfer is irreversible and the energy is then damped by viscosity in the membrane. On the time-frequency diagrams, we can see the resonance capture that the membrane M_1 only leaves when the acoustic level reaches zero, which avoids the return of the energy. After that, due to the energy-frequency dependence of a cubic oscillator, the frequency of the membrane decreases with its amplitude, until it reaches its first resonance frequency (59 Hz). After the cancellation of the sound, the frequency of the membrane M_2 follows passively the same variation than the frequency of membrane M_1 , as it is then the last vibrating element in the system.
- $\mathcal{A} > S_2^{M_2}$ (Fig. 4(c)) : beyond the second threshold of the second membrane M_2 , both membranes are initially activated on the resonance capture with the acoustic medium. The decrease is then still linear, but much faster. The presence of the second membrane allows a stronger targeted energy transfer if the initial energy is high enough. Note that below a certain acoustic level, during the decrease, the membrane M_2 stops acting, leaving the membrane M_1 proceeding the end of the transfer. The slope becomes then the same than before, corresponding to the previous case where a single membrane is active.

The Fig. 5 summarizes these steps showing the positive envelopes of the sound pressure time series for all initial conditions. It provides an alternative illustration of the difference between the three cases described above.

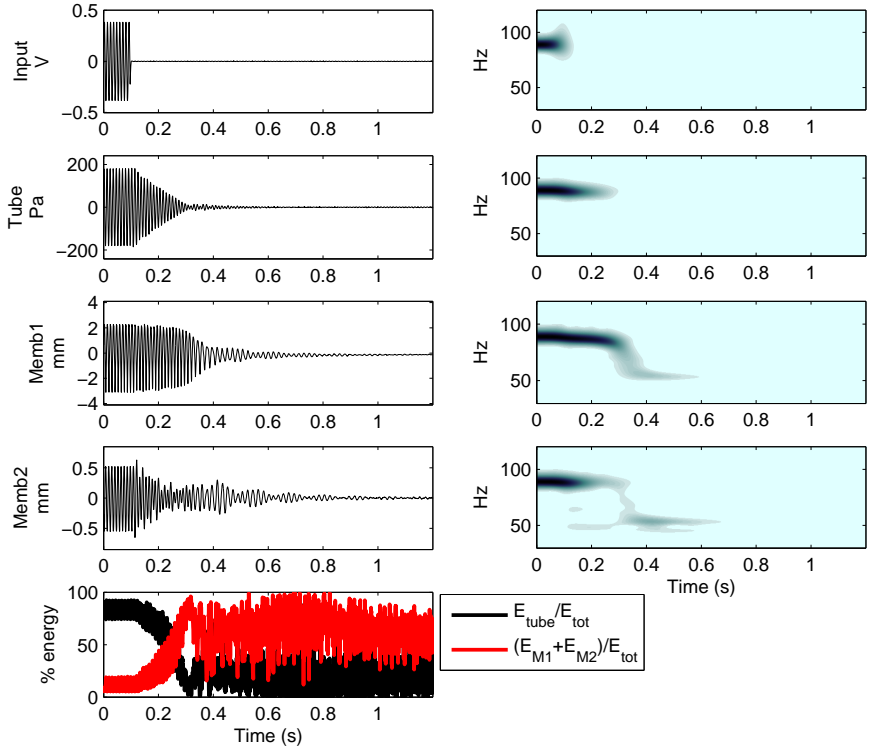
The successive activation of the membranes thus does not change much about the overall mechanism of targeted energy transfer, just making it more and more intense each time an additional membrane is activated. This additive mechanism is similar to what was obtained analytically in reference [22] (equation 4.51) for the case of a nongrounded configuration with several nonlinear absorbers in parallel.

2.4. Frequency responses

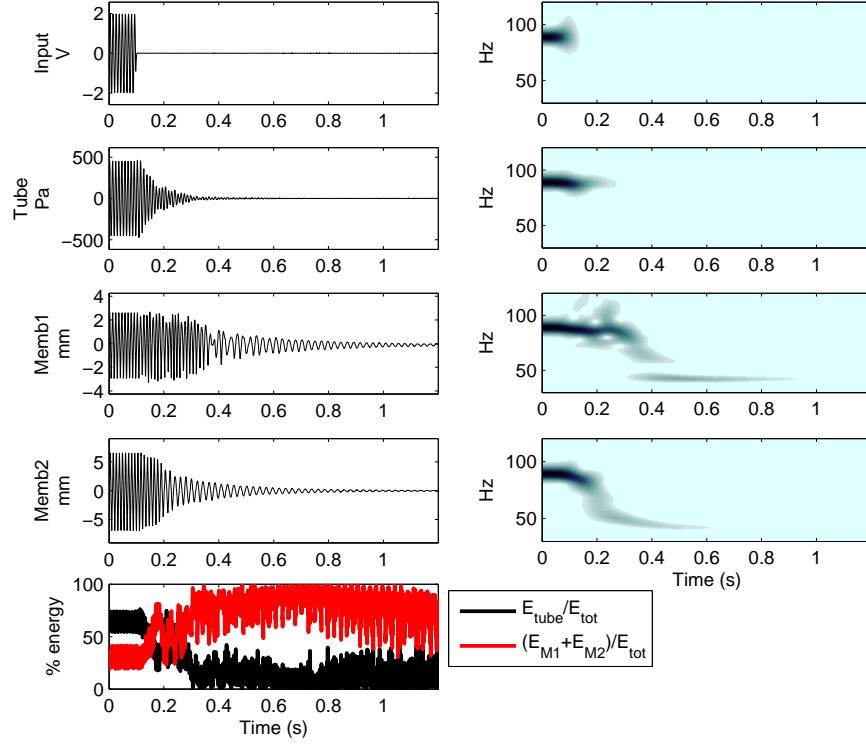
This section finally deals with the influence of both membranes on the frequency responses of the acoustic medium. These responses have been measured with a swept



(a) $\mathcal{A} = 0.12$ V.



(b) $\mathcal{A} = 0.4$ V.



(c) $\mathcal{A} = 2 \text{ V}$.

Figure 4: *Experimental results*. Free oscillations of the system after different initial conditions. From top to bottom: input signal, acoustic pressure at the middle of the tube, displacement of the center of the membrane M_1 , displacement of the center of the membrane M_2 and percentage of energy in the tube and in the membranes. On the right: wavelet transforms of the corresponding times series of the left side.

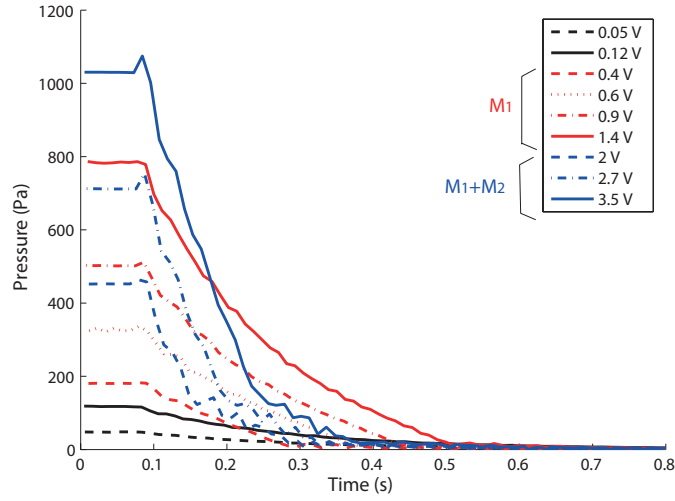


Figure 5: *Experimental results*. Positive envelopes of the sound pressure time series for all initial conditions.

sine source at constant amplitude. Five of them, corresponding to the five types of responses observed depending on the input level, are plotted in Fig. 6:

- $\mathcal{A} = 0.1$ V: for low input levels, none of the two membranes is never activated and the response simply follows the first resonance peak of the acoustic medium.
- $\mathcal{A} = 0.18$ V: for levels between $S_1^{M_1}$ and $S_2^{M_1}$, i.e. high enough to observe the quasi-periodic regime of the membrane M_1 , the resonance peak of the acoustic medium is clipped. This clipping is only due to the action of the first membrane, the level being too low for the membrane M_2 to act.
- $\mathcal{A} = 0.8$ V: for levels between $S_2^{M_1}$ and $S_1^{M_2}$, the frequency response has a new resonance peak slightly shifted to lower frequencies and whose maximal amplitude is slightly lower than the original peak. Along this peak, the membrane M_1 is activated, vibrates in phase with the acoustic displacement of the air at the end of the tube and acts as an additional mass on the system, whereas the membrane M_2 is still inactive, the level being still too weak for that membrane. These first three types of frequency responses are the same than what we have seen in the previous paper [19], since for now only one membrane is active.
- $\mathcal{A} = 1.5$ V: for levels between $S_1^{M_2}$ and $S_2^{M_2}$, the membrane M_2 is activated and its quasiperiodic regime allows to clip this last second resonance peak. The membrane M_2 acts independently, on the resonance peak of a global system (acoustic medium and membrane M_1).
- $\mathcal{A} = 3$ V: for very high input levels, above $S_2^{M_2}$, a third resonance peak is observed, still more shifted to lower frequencies and whose maximal amplitude a little lower again. Along this peak, both membranes are activated and vibrate in phase with the acoustic displacement of the air at the end of the tube.

In summary, we are still attending the successive action of the membranes that are activated one after the other, when the input level increases. They act independently of each other, each time repeating the same process, having an influence only on the resonance peak that they “see”, creating a succession of clipping and new shifted resonance peaks, one membrane clipping the peak created by the previous one. There is no negative correlation effects, and this addition of NES can be seen as a way to enlarge the useful range of a TET system.

3. Extension for more membranes thanks to numerical simulations

The earlier model, which corresponds to a set-up with two membranes, can be extended to a n membranes set-up. The resulting system is then:

$$\begin{aligned}
m_a \ddot{u}_a + c_f \dot{u}_a + k_a u_a + S_t k_b (S_t u_a - \sum_{j=1}^n \frac{S_j}{2} q_j) &= F \cos(\Omega t) \\
m_1 \ddot{q}_1 + k_{11} [(\frac{f_{11}}{f_{01}})^2 q_1 + \eta \dot{q}_1] + k_{31} [q_1^3 + 2\eta q_1^2 \dot{q}_1] + \frac{S_1}{2} k_b (\sum_{j=1}^n \frac{S_j}{2} q_j - S_t u_a) &= 0 \\
\dots
\end{aligned}$$

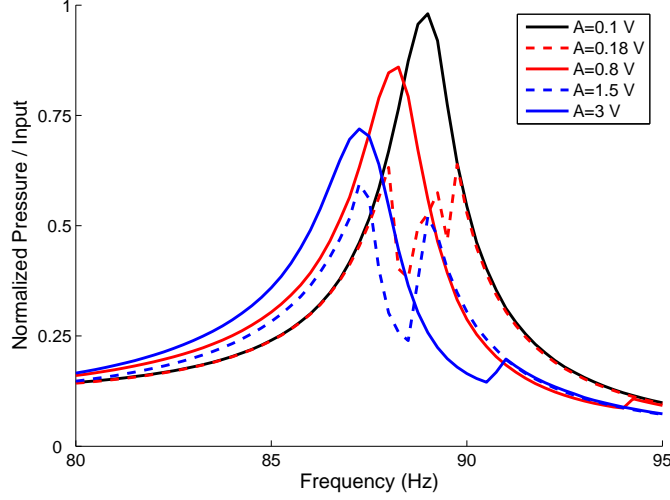


Figure 6: *Experimental results.* Frequency responses of the acoustic environment coupled to two membranes for different input amplitudes.

$$\begin{aligned}
& m_i \ddot{q}_i + k_{1i} \left[\left(\frac{f_{1i}}{f_{0i}} \right)^2 q_i + \eta \dot{q}_i \right] + k_{3i} [q_i^3 + 2\eta q_i^2 \dot{q}_i] + \frac{S_i}{2} k_b \left(\sum_{j=1}^n \frac{S_j}{2} q_j - S_t u_a \right) = 0 \\
& \dots \\
& m_n \ddot{q}_n + k_{1n} \left[\left(\frac{f_{1n}}{f_{0n}} \right)^2 q_n + \eta \dot{q}_n \right] + k_{3n} [q_n^3 + 2\eta q_n^2 \dot{q}_n] + \frac{S_n}{2} k_b \left(\sum_{j=1}^n \frac{S_j}{2} q_j - S_t u_a \right) = 0 \\
& \text{with } m_a = \frac{\rho_a S_t L}{2}, \quad m_i = \frac{\rho_m h S_i}{3}, \quad k_b = \frac{\rho_a c_0^2}{V_2}, \quad k_a = \frac{\rho_a S_t c_0^2 \pi^2}{2L} \\
& k_{1i} = \frac{1.015^4 \pi^5}{36} \frac{E h_i^3}{(1 - \nu^2) R_i^2}, \quad k_{3i} = \frac{8\pi E h_i}{3(1 - \nu^2) R_i^2} \\
& f_{0i} = \frac{1}{2\pi} \sqrt{\frac{1.015^4 \pi^4}{12} \frac{E h_i^2}{(1 - \nu^2) \rho_m R_i^4}}, \quad S_i = \pi R_i^2
\end{aligned}$$

The simulations with two membranes showed the same phenomena as those observed experimentally, with an agreement similar to what we observed so far with a single membrane set-up in the paper [19]. In order to extend and generalize the previous results to a n membranes set-up, we used this model and performed numerical simulations of the frequency responses for two configurations with four membranes, one with clearly different membranes and another with quasi-identical membranes.

3.1. The case of four clearly different membranes

The configurations of the membranes were chosen so that they have significantly different thresholds and in a well known order (see Table 1).

The results of these simulations are shown in Fig. 7 where it appears that the mechanism observed experimentally remains similar and is simply extended to the case of four membranes:

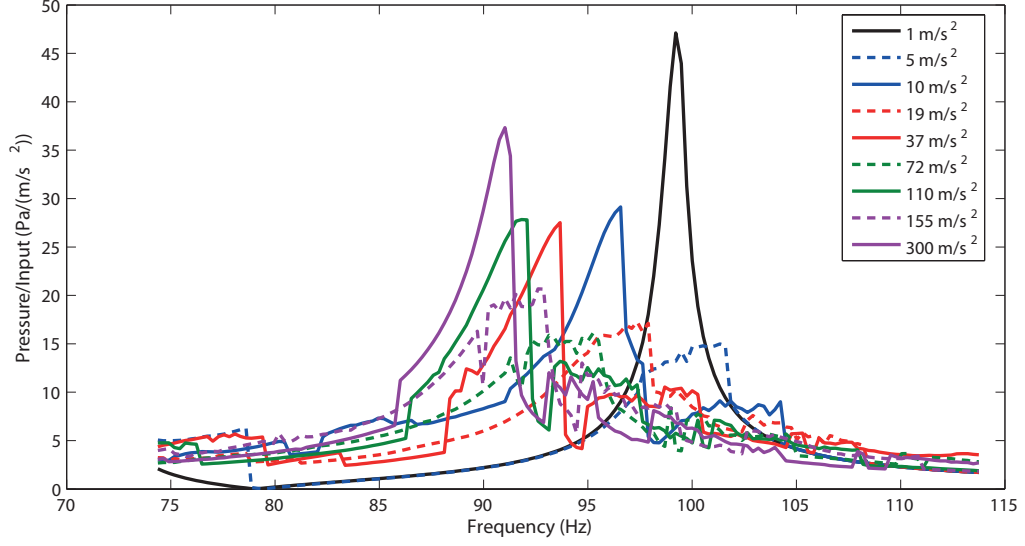


Figure 7: *Numerical results.* Frequency responses with four different membranes for nine different input levels.

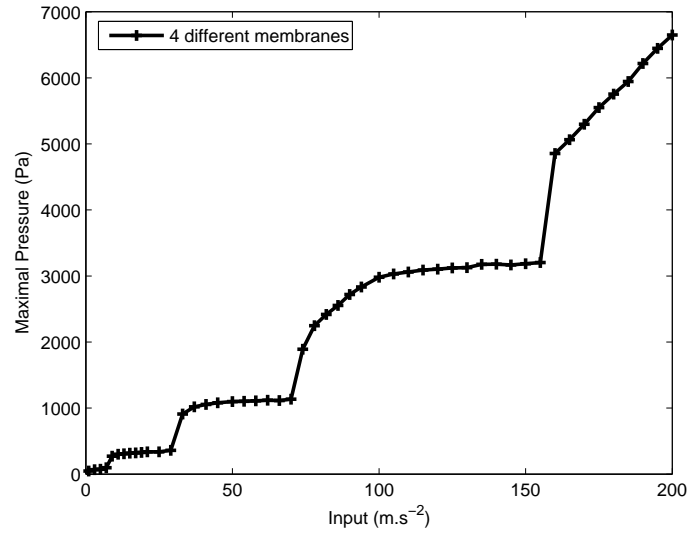


Figure 8: *Numerical results.* Curve connecting the maxima of each frequency response for a configuration with four different membranes in parallel.

Membrane	R_i (mm)	h_i (mm)	f_{1i} (Hz)	η_i (s)
M_1	20	0.2	50	0.00025
M_2	30	0.3	40	0.00025
M_3	40	0.4	30	0.00025
M_4	50	0.5	20	0.00025

Table 1: Configurations of the four different membranes. R_i , h_i , f_{1i} , η_i are respectively the radius, thickness, first resonance frequency and damping factor of the membrane M_i .

- For a very low input level, the frequency response follows the original peak of the acoustic medium.
- From a certain input level, this peak is clipped by the first membrane while all others remain inactive.
- Increasing the input level creates a new resonance peak slightly shifted to lower frequencies.
- The same process is observed whenever a new membrane is activated: when the input level allows to activate an additional membrane, this enables a clipping of the last created peak, then a new peak, each time shifted to lower frequencies, appears increasing again the input level.

So we observe in Fig. 7 nine different frequency responses, corresponding to nine different input levels: the original peak, the original peak clipped by M_1 , the peak of the system $\{\text{tube}+M_1\}$, the peak of the system $\{\text{tube}+M_1\}$ clipped by M_2 , the peak of the system $\{\text{tube}+M_1+M_2\}$, the peak of the system $\{\text{tube}+M_1+M_2\}$ clipped by M_3 , the peak of the system $\{\text{tube}+M_1+M_2+M_3\}$, the peak of the system $\{\text{tube}+M_1+M_2+M_3\}$ clipped by M_4 and finally the peak of the system $\{\text{tube}+M_1+M_2+M_3+M_4\}$.

The Fig. 8 presents the curve connecting the maxima of each frequency response, each point showing the maximal pressure level observed for a certain input level. This curve highlights different horizontal zones, where a certain membrane acts as a nonlinear energy sink, preventing the acoustic level to exceed the level where this membrane gets activated. As the four membrane configurations are very different, these zones are here clearly separated and independent.

3.2. The case of several very similar membranes

In order to study the interest of using several very similar membrane, we performed different simulations of the behavior of the system with one, two, three and four membranes in parallel, whose configurations were chosen as mentioned in Table 2.

The results of this study are shown in the Fig. 9 where the curves of maximal acoustic level depending on the input level are plotted for these four different configurations. This figure shows that the horizontal zone where the targeted energy transfer exists can be extended thanks to an additional similar membrane. In each situation where we simulated several membranes, we could have replaced them with a single one. But this last membrane should have had properties unavailable in practice. As one of the most important drawbacks of nonlinear absorbers is to act only

Membrane	R_i (mm)	h_i (mm)	f_{1i} (Hz)	η_i (s)
M_1	30	0.3	40	0.00025
M_2	31	0.31	40	0.00025
M_3	32	0.32	40	0.00025
M_4	33	0.33	40	0.00025

Table 2: Configurations of the four very similar membranes. R_i , h_i , f_{1i} , η_i are respectively the radius, thickness, first resonance frequency and damping factor of the membrane M_i .

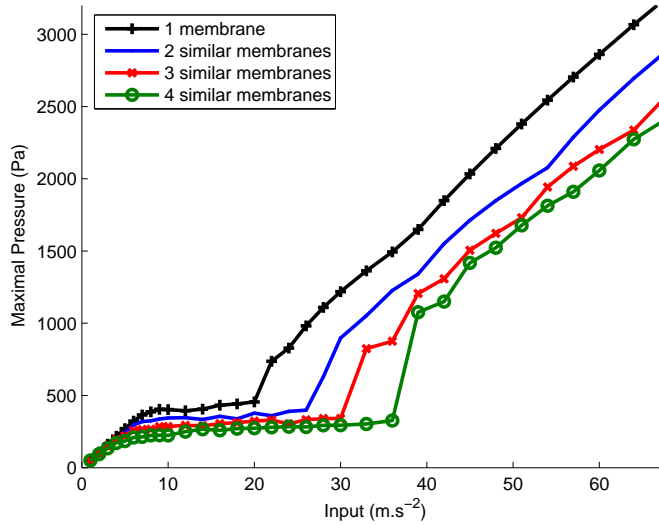


Figure 9: *Numerical results.* Curves connecting the maxima of each frequency response for four different configuration: a configuration with only one membrane, and three other configurations with one, two and three additional and very similar membranes in parallel.

in a restricted zone, that is to say between two energy thresholds, the possibility of extending this zone is a very important result.

4. Conclusion

Based on the set-up of the previous paper [19], this mainly experimental study of targeted energy transfer in acoustics thanks to two nonlinear membranes absorbers in parallel showed, in both temporal and frequency aspects, that the use of several NES is a way to extend the energy range and the efficiency of TET. This is done thanks to an additional effect of the different membranes, which are activated in turn and behave relatively independently, repeating several times the same phenomena as those we know for a single nonlinear absorber set-up. Thanks to a model and numerical simulations, we could extend and generalize this results to a higher number of parallel absorbers: an addition of different membranes creates a new zone of TET and an addition of similar ones extends the existing zone of TET. Since previous works about multiple NES only deal with a series coupling, because of specific constraints that are not existing in our acoustic case (mechanical systems in which the absorber is in a nongrounded configuration), this paper brings new

information in this growing field of nonlinear absorbers, where acoustics has different properties than mechanical engineering applications of TET.

Acknowledgement

This research was supported by French National Research Agency in the context of the ADYNO project (ANR-07-BLAN-0193).

References

- [1] O. Gendelman, L. Manevitch, A. Vakakis, R. M'Closkey, Energy pumping in nonlinear mechanical oscillators: Part I - Dynamics of the underlying hamiltonian systems, *Journal of Applied Mechanics* 68 (2001) 34–41.
- [2] A. Vakakis, O. Gendelman, Energy pumping in nonlinear mechanical oscillators: Part II - Resonance capture, *Journal of Applied Mechanics* 68 (2001) 42–48.
- [3] A. Vakakis, Inducing passive nonlinear energy sinks in vibrating systems, *Journal of Vibration and Acoustics* 123 (2001) 332.
- [4] A. Vakakis, L. Manevitch, O. Gendelman, L. Bergman, Dynamics of linear discrete systems connected to local, essentially non-linear attachments, *Journal of Sound and Vibration* 264 (2003) 559–577.
- [5] A. Vakakis, R. Rand, Non-linear dynamics of a system of coupled oscillators with essential stiffness non-linearities, *International Journal of Non-Linear Mechanics* 39 (2004) 1079–1091.
- [6] A. Vakakis, L. Manevitch, A. Musienko, G. Kerschen, L. Bergman, Transient dynamics of a dispersive elastic wave guide weakly coupled to an essentially nonlinear end attachment, *Wave Motion* 41 (2005) 109–132.
- [7] F. Georgiades, A. Vakakis, G. Kerschen, Broadband passive targeted energy pumping from a linear dispersive rod to a lightweight essentially non-linear end attachment, *International Journal of Non-Linear Mechanics* 42 (2007) 773–788.
- [8] P. Panagopoulos, A. Vakakis, S. Tsakirtzis, Multi-scaled analysis of the damped dynamics of an elastic rod with an essentially nonlinear end attachment, *International Journal of Solids and Structures* 41 (2004) 6505–6528.
- [9] P. Panagopoulos, F. Georgiades, S. Tsakirtzis, A. Vakakis, L. Bergman, Multi-scaled analysis of the damped dynamics of an elastic rod with an essentially nonlinear end attachment, *International Journal of Solids and Structures* 44 (2007) 6256–6278.
- [10] F. Georgiades, A. Vakakis, Dynamics of a linear beam with an attached local nonlinear energy sink, *Communications in Nonlinear Science and Numerical Simulation* 12 (2007) 643–651.
- [11] F. Georgiades, A. Vakakis, Passive targeted energy transfers and strong modal interactions in the dynamics of a thin plate with strongly nonlinear attachments, *International Journal of Solids and Structures* 46 (2009) 2330–2353.
- [12] L. Manevitch, O. Gendelman, A. Musienko, A. Vakakis, L. Bergman, Dynamic interaction of a semi-infinite linear chain of coupled oscillators with a strongly nonlinear end attachment, *Physica D* 178 (2003) 1–18.
- [13] E. Gourdon, N. Alexander, C. Taylor, C. Lamarque, S. Pernot, Nonlinear energy pumping under transient forcing with strongly nonlinear coupling: Theoretical and experimental results, *Journal of Sound and Vibration* 300 (2007) 522–551.
- [14] F. Nucera, F. Lo Iacono, D. McFarland, L. Bergman, A. Vakakis, Application of broadband nonlinear targeted energy transfers for seismic mitigation of a shear frame: Experimental results, *Journal of Sound and Vibration* 313 (2008) 57–76.
- [15] Y. Lee, A. Vakakis, L. Bergman, D. McFarland, G. Kerschen, Suppression of aeroelastic instabilities by means of targeted energy transfers: Part I, theory, *AIAA Journal* 45 (3) (2007) 693–711.
- [16] Y. Lee, G. Kerschen, D. McFarland, W. Hill, C. Nickkawde, T. Strganac, L. Bergman, A. Vakakis, Suppression of aeroelastic instability by means of broadband TET: Part II, experiments, *AIAA Journal* 45 (2007) 2391–2400.

- [17] R. Vigié, G. Kerschen, J.-C. Golinval, D. McFarland, L. Bergman, A. Vakakis, N. van de Wouw, Using passive nonlinear targeted energy transfer to stabilize drill-string systems, *Mechanical Systems and Signal Processing* 23 (2009) 148–169.
- [18] B. Cochelin, P. Herzog, P.-O. Mattei, Experimental evidence of energy pumping in acoustics, *C. R. Mecanique*.
- [19] R. Bellet, B. Cochelin, P. Herzog, P.-O. Mattei, Experimental study of targeted energy transfer from an acoustic system to a nonlinear membrane absorber, *Journal of Sound and Vibration* 329 (2010) 2768–2791.
- [20] E. Gourdon, C. Lamarque, Energy pumping for a larger span of energy, *Journal of Sound and Vibration* 285 (2005) 711–720.
- [21] Y. Lee, A. Vakakis, L. Bergman, D. McFarland, G. Kerschen, Enhancing robustness of aeroelastic instability suppression using MDOF energy sinks, *AIAA Journal* 46 (6) (2008) 1371–1394.
- [22] T. Nguyen, Etude du comportement dynamique et optimisation d’absorbeurs nonlinéaires : théorie et expérience, Thèse de l’Ecole Centrale de Lyon, 2010.